International Journal of Bioprinting

RESEARCH ARTICLE

3D printing biocompatible materials with Multi Jet Fusion for bioreactor applications

Balasankar Meera Priyadarshini[1†], Wai Kay Kok[1†], Vishwesh Dikshit[1], Shilun Feng[2,3], King Ho Holden Li[4*], Yi Zhang[1]

[1]HP-NTU Digital Manufacturing Corporate Lab, Nanyang Technological University, 639798, Singapore

[2]State Key Laboratory of Transducer Technology, Shanghai Institute of Microsystem and Information Technology, Chinese Academy of Sciences, Shanghai, 200050, China

[3]School of Electrical and Electronic Engineering, Nanyang Technological University, 639798, Singapore

[4]School of Mechanical and Aerospace Engineering, Nanyang Technological University, 639798, Singapore

Abstract

In the evolving three-dimensional (3D) printing technology, the involvement of different materials in any new 3D printing process necessitates a thorough evaluation of the product's biocompatibility for biomedical application. Here, we examined the ability of Multi Jet Fusion (MJF)-printed PA-12 to support cell proliferation and osteogenesis. Our results show that leachate from MJF-printed PA-12 does not inhibit the growth of L929 fibroblast and MC3T3e1 osteoblast. The substrate supports the attachment and proliferation of both cell types, though not at a level comparable to conventional polystyrene culture plate. Neither plasma treatment, poly-D-lysine, nor collagen coatings narrowed the gap substantially, suggesting the possible influence of other limiting factors. The substrate can also support MC3T3e1 osteogenesis. However, MJF-printed PA-12 exhibits varying ability in supporting the proliferation of different cell types, especially in subsequent passages. While L929's proliferation is comparable from passage-to-passage, MC3T3e1's growth ability is noticeably compromised. Interestingly, our results show that L929 subcultured back to polystyrene plate retains the ability to grow as robustly as those on the conventional plate, suggesting that MJF-printed PA-12 does not permanently impair cell proliferation. In addition, we have shown the successful culture of bacterial *Escherichia coli* on MJF-printed PA-12. Together, our study demonstrated the potential of MJF-printed PA-12 for biological applications.

Keywords: 3D printing; PA-12; Nylon; Multi Jet fusion; Cell culture; Bacteria fouling; Protein fouling; Bioreactors

†These authors contribute equally to this work.

***Corresponding author:**
King Ho Holden Li
(holdenli@ntu.edu.sg)

Citation: Priyadarshini BM, Kok WK, Dikshit W, *et al*., 2023, 3D printing biocompatible materials with Multi Jet Fusion for bioreactor applications. *Int J Bioprint*, 9(1): 623.
https://doi.org/10.18063/ijb.v9i1.623

Received: April 13, 2022
Accepted: July 01, 2022
Published Online: October 22, 2022

1. Introduction

Three-dimensional (3D) printing has presented new opportunities for advanced manufacturing of a wide spectrum of materials such as metals, ceramics, composites, smart materials, as well as combinations of these materials, due to its innate ability of

easy customization, scalability, rapid manufacturing, and material tuning[1-4]. Polymer-based material systems are widely adopted by 3D printing for their abundant availability, unparalleled multifunctionality, and versatility associated with processability and performance[5,6]. The range of polymers used in 3D printing encompasses thermoplastics, thermosets, functional polymers, polymer blends, composite elastomers, and hydrogels[7-9]. For instance, 3D printing techniques, such as fused deposition modeling (FDM), material jetting, and selective laser sintering (SLS) use thermoplastics, while stereolithography (SLA) and direct ink writing use photocurable thermosetting polymers[10,11]. 3D printing has improved material properties and enhanced the functionality of the printed construct[12-14].

3D printing has emerged as an effective tool for many biomedical applications such as biocompatible implants, 3D organ models and organoids, drug delivery, and tissue regeneration[15-17]. Considerable effort has been dedicated toward 3D printing of bioreactors, which provide an opportunity to design and construct intricate, custom-made designs with well-defined architectures[18]. The biocompatibility of a 3D-printed bioreactor influences its role in the sustenance of cell functions. At times, the printed material may not be conducive for cell growth. Many studies have documented *in vitro* cellular inhibition due to the toxic residues in solidified polymers post-printing[19-22], while some have attempted to mitigate such effects by developing post-printing treatment such as ultraviolet light exposure[23,24]. Some 3D-printed *in vivo* devices have been shown to cause infections and allergic responses in patients[25,26]. Therefore, it is important to examine biocompatibility of 3D-printed materials to minimize the effect of failure in their performance as 3D-printed bioreactors.

Selecting the optimal printing technique and material is imperative to maximizing the chance of success of a 3D printing process. Several bioreactors have been 3D-printed by FDM due to its low cost, high speed, simplicity and capability of printing various biomaterials, or by SLS which demonstrated good isotropic mechanical properties with complex geometries, and required no support[27-29]. Other methods such as SLA and its variants, namely, projection micro SLA, showed a very good resolution, accuracy, and printing time independent of the complexity of designs[30-32]. Commonly used polymer materials for 3D printing include acrylonitrile butadiene styrene, poly(caprolactone) (PCL), poly(D,L-lactic acid-co-glycolic acid) (PLGA), poly ether ester ketone, polylactic acid, polycarbonate, polyetherimide, and nylon[8,10,33], and the selection of material depends on the application of the end product[34]. For example, PCL is commonly utilized by FDM and SLS for tissue engineering applications, whereas FDA-approved PLGA copolymers are used by FDM to print parts for clinical use. Nylon can be 3D-printed using FDM, SLS, and Multi Jet Fusion (MJF), and it is best suited for industrial and engineering applications[35].

Powder bed fusion (PBF) is a promising 3D printing technique that offers high-throughput manufacturing of biocompatible bioreactors[17,36]. SLS and MJF, two most popular PBF 3D printing technologies, have attracted considerable attention from academic and industrial organizations due to their rapid printing speed and compatibility with a variety of polymer materials[37,38]. Many SLS-printed polymer (such as PCL and PLLA) 3D constructs were evaluated for biocompatibility due to their ability to promote cell adhesion and support cell differentiation[39,40]. Other non-toxic materials such as thermoplastic polyurethane and polyamide nylon 12 (PA-12) were also printed by SLS for different bioapplications[41-43]. With a continuous influx of new printable materials, it is important to understand both the advantages and limitations of the new printing technologies and materials.

MJF is an innovative 3D printing technique developed by Hewlett-Packard (HP) that works similar to a binder jet technique in using a powder delivery system. However, the unique build style includes incorporation of a multi-agent inkjet system within the PBF process and makes it different from other PBF technologies[43,44]. The printing process involves the application of a thin layer of powder materials on the build plate followed by selective deposition of the fusing agent onto areas, where the powder particles are intended to fuse, and the addition of detailing agent at the contour of the patterns to create smooth surfaces. The powder layer on exposure to the infrared energy source allows the area of the fusion agent to fuse and forms the part. This technique is capable of fabricating parts with excellent dimensional precision and low porosity[45].

A recent evaluation of mechanical properties and printing characteristics suggest that MJF-printed specimens have a better surface finish, high strength, and wear resistance strength than SLS-printed counterparts[43]. In addition, MJF printing has also shown the least impact on the environment and human health, allowing for concurrent fabrication of different designs and large-scale green manufacturing compared to other technologies[35].

PA-12 is an inexpensive, bio-based, non-toxic, and semi-crystalline polymer for sustainable 3D printing. It offers outstanding impact resistance, good resolution, strong chemical resistance, thermal stability, durability, and lowest moisture absorbance of all the polyamides[46,47]. Due to its mechanical properties and excellent biocompatibility

with human bone cell and tissue types, PA-12 has been used as a non-degradable biomaterial[48,49]. Several studies have reported the use of PA 11/12 for SLS printing[50]. However, few studies have explored the potential of developing biocompatible 3D-printed PA-12 bioreactors using MJF. As MJF-printing differs from SLS and other methods, we cannot assume that MJF-printed PA-12 possesses the same features or properties that make it equally biocompatible. Studies have shown that carbon black nanoparticle and triethylene glycol at high concentration are toxic to cells[51,52]. These are components of fusing and detailing agents used in MJF printing. Hence, it is uncertain if the fusing and detailing agents in PA-12 after printing are similarly cytotoxic to cells. Although MJF produces good feature resolution, the printed surface is still rough and irregular. It is unknown how such surface topography will affect cell adhesion, morphology, and other anchorage-dependent cellular processes. As cellular behavior can be manipulated by extracellular matrix, the affinity of MJF-printed PA-12 for protein biomolecules needs to be assessed. Ease of functionalization of PA-12 allows cell adhesion to be enhanced or manipulated.

It is, therefore, the aim of this study to address these issues posed by the unique features or properties of MJF-printed PA-12. We investigate the suitability of MJF-printed PA-12 as a cell support for potential applications such as bioreactors. To test that, we culture mammalian fibroblasts and osteoblasts on PA-12 cell culture chambers 3D-printed by MJF and check how cells tolerate being directly cultivated in these MJF-printed cell culture chambers. In addition, the effect of material leachate on the cultured cells are also tested by exposing the cells to the leachate of PA-12 printed by MJF. The effect of various surface coating and modification of MJF-printed PA-12, such as collagen and poly-D-lysine (PDL) coating or O_2 plasma-treatment, are studied. In addition, the microbial growth and adhesion on 3D-printed PA-12 are also examined. We find that MJF-printed PA-12 cell culture chambers are non-cytotoxic and support the growth of both mammalian and bacterial cells. We also find out that 3D-printed PA-12 has varied ability to support different cell types. This study lays the groundwork for the potential use of MJF-printed PA-12 cell culture chambers as bioreactors.

2. Materials and methods

2.1. Fabrication, processing, and sterilization of 3D-printed PA-12 cell culture chambers

The PA-12 cell culture chamber printed by MJF is shown in Figure 1A. The dimension of the printed PA12 cell culture chambers is 1.75 mm wall thickness, 16 mm inner diameter, and 5 mm depth. This gives the chamber a surface area of about 1.9 cm^2, similar to each well in a 24-wells polystyrene plate. All cell culture chambers were manufactured using HP MJF 5200 3D-printer. HP proprietary fusing agent (containing 5.2% carbon black suspended in a solution of 65% water, 18.7% 2-pyrollidone, and 8.4% triethylene glycol) and detailing agent (containing mostly 85% water, 3.7% 2-pyrollidone, and 11.1% triethylene glycol)[53,54] were used. HP 3D High-Reusability (HR) PA-12 powder was used to print the cell reaction chamber. The printing was done on the "Balanced" print mode and new/reused powder mixture ratio was maintained at 20:80. After printing, the print bed was allowed to cool to room temperature before the printed parts were retrieved.

To examine the effect of the fusing and detailing agents on the surface morphology and composition, specimens without the detailing and fusing agents were fabricated by melting and casting HP 3D HR PA-12 powder into a 24 mm length × 24 mm width × 10 mm height block using a convection oven (220°C, 2h and normal cooling). Then, a 16 mm blind hole was milled at a depth of 10 mm (Figure 1B).

Following the fabrication, the 3D-printed and casted PA-12 cell culture chambers were cleaned with distilled water in an ultrasonic bath for 20 min. The cell culture chambers were then soaked in 70% ethanol at 4°C for 5 min, washed, dried in an oven at 60°C for ~2 h, and then used for subsequent experiments.

2.2. Surface characterization of 3D-printed PA-12 cell culture chambers

2.2.1. Surface morphology

The surface texture and morphology of the casted pure PA-12 and 3D-printed PA-12 were observed using Scanning Electron Microscopy (SEM). Specimens were fixed on metal stubs using double-sided carbon tape, gold sputter coated (BALTEC, SCD 005 Sputter Coater, Scotia, NY, USA), and scanned at an accelerating voltage of 10 keV using JEOL JSM-5500LV (Japan) (n = 3).

2.2.2. Surface roughness

The optical appearance of the surface and average surface roughness (R_a) of the pure cast PA-12 and 3D-printed PA-12 were measured using confocal laser scanning microscopy (Keyence Laser Scanning Confocal Microscope VK-X200 series). Surface roughness measurements were taken from three random locations on the specimens (n = 3).

2.2.3. Protein fouling

The ability of the 3D-printed PA-12 to adsorb proteins was studied by exposing the surface to bovine serum albumin labeled with FITC (BSA-FITC). Both untreated and O_2

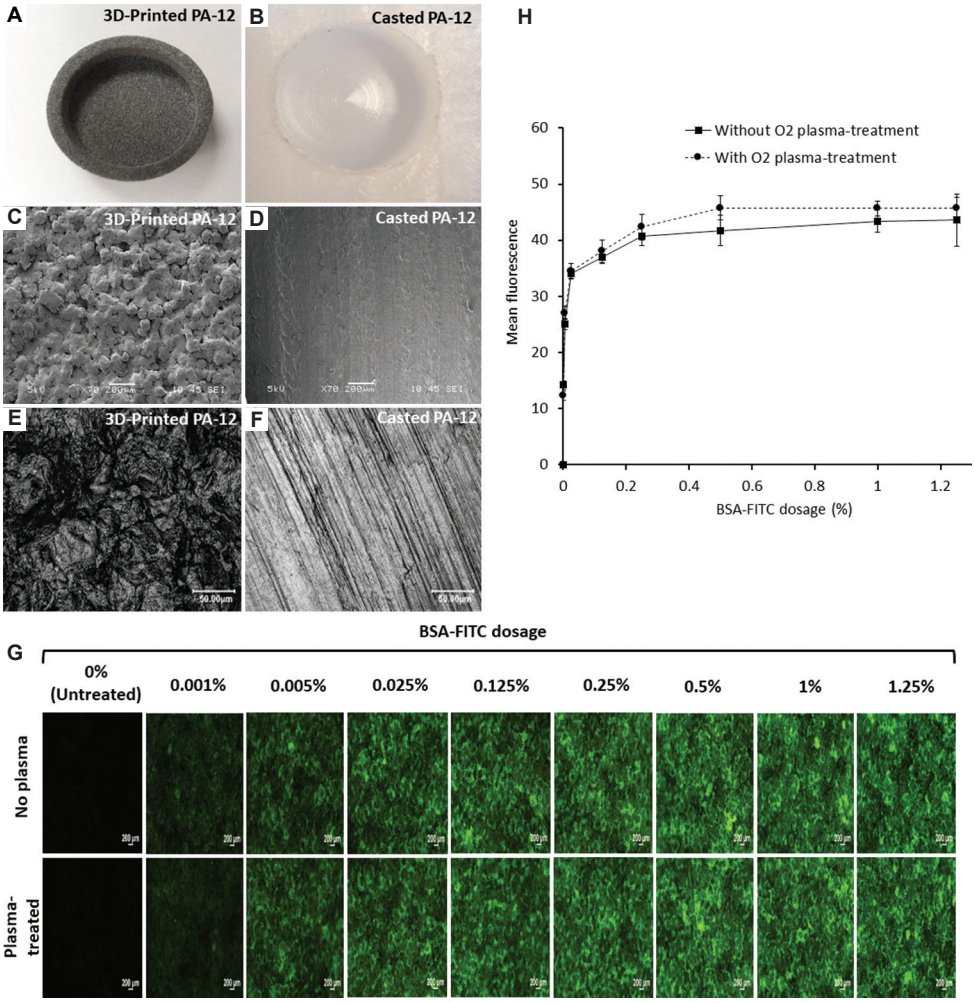

Figure 1. Picture of a (A) 3D-printed PA-12 and (B) casted PA-12 cell culture chamber. Scanning electron microscopy images showing the surface morphology of (C) 3D-printed PA-12 and (D) pure casted PA-12, respectively (scale bar: 200 µm). Representative confocal scanning microscopy images displaying the surface roughness of (E) 3D-printed PA-12 and (F) pure casted PA-12, respectively (scale bar: 50 µm). (G) Fluorescence microscopy images of increasing concentrations of BSA-FITC conjugate bound on 3D-printed PA-12 substrates with and without O_2 plasma-treatment. (H) Standard curve showing fluorescence signal quantification of BSA-FITC bound to 3D-printed PA-12 substrates with and without O_2 plasma-treatment.

plasma-treated cell culture chambers were used. BSA-FITC (#A23015, Thermofisher, USA) of eight concentrations at 0% (blank), 0.001%, 0.005%, 0.025%, 0.125%, 0.25%, 0.5%, 1%, and 1.25% were prepared in phosphate-buffered saline (PBS). 50 µL of each dosage was added to cover a surface area of 31.65 mm^2 of each O_2 plasma-treated (Harrick Plasma Cleaner PDC-002, 230 vac, 50 Hz) and untreated cell culture chamber and incubated for 1 h. The wells were, then, washed thrice with PBS and air-dried before being viewed under a fluorescence microscope (Nikon Eclipse Ci-S, 100-240V, 0.8A, 50/60 Hz). Images of four different fields of each well were taken. Signal intensity was quantified using ImageJ 1.52a (Java 1.8.0_112). The average signal intensity of each dosage was used to plot the binding curves.

2.2.4. Contact angle

The surface hydrophilicity of 3D-printed PA-12 cell culture chambers was assessed by measuring the water contact angle (Optical Contact Angle OCA35, Dataphysics, Germany) using the sessile drop method at room temperature (n = 3 per group). Cell culture chambers were O_2 plasma-treated, and surface coated with PDL and collagen (CLG) (50 µg/mL) to ensure if O_2 plasma-treatment and coatings were beneficial. Uncoated cell culture chambers were used as control. A water droplet was placed on the substrate surface and contact angle was measured after 10 s.

2.3. Biocompatibility evaluation

The *in vitro* biocompatibility of the 3D-printed cell culture chamber was tested by directly culturing mammalian

fibroblasts and osteoblasts under conditions pertaining to short-term (day 2 and day 4) and long-term (day 28) culture. Moreover, long-term studies were also conducted to investigate the effect of two rounds of subculture on the viability of cells on 3D-printed cell culture chambers. The 24-well plates with a similar surface area as the printed PA-12 chambers were used as the comparison basis for assessing the printed chamber's biocompatibility in all assays throughout the study.

2.3.1. Cell culture conditions

Murine L929 fibroblasts were cultured in DMEM supplemented with 10% fetal bovine serum (FBS) and 1% penicillin/streptomycin. MC3T3e1 mouse osteoblasts were propagated in α-MEM supplemented with 10% FBS and 1% penicillin/streptomycin. All cell culture reagents were obtained from Gibco, USA. Both cell lines were maintained at 37°C in a humidified incubator supplied with 5% CO_2. For all experiments, fibroblasts and osteoblasts were seeded at a density of 5000 and 4000 cells/cm^2 at day 0, respectively, and allowed to grow to confluence for 4 days.

2.3.2. Effect of PA-12 leachate

The effect of substance leachate from 3D-printed PA-12 on cell adherence and viability was determined by culturing cells in the leachate medium. The leachate medium was prepared by soaking fourteen 3D-printed PA-12 cell culture chambers (weight = 1.344 g ± 0.02 per chamber; total surface area of the cup: 452.388 mm^2) in respective culture medium (~30 mL) for 5 days at 37°C, filtered and used for cell culture. Here, cells were grown in normal and leachate medium on 24-well plates, tested for cell adherence and viability by performing MTT assay and fluorescence microscopy (n = 4 per group).

For fluorescence microscopy, Alexa Fluor® 546 phalloidin (#A22283, Thermofisher, USA) was used to stain actins, while Hoechst 33342 (Sigma-Aldrich, USA) was used as a counterstain to visualize the nuclei. Briefly, cells were fixed with 4% paraformaldehyde, washed with ×1 PBS, and permeabilized with 0.1% Triton-X for 15 min. Cells were then stained with Alexa Fluor® 546 phalloidin for 1 h and counterstained with Hoechst 33342 for 10–15 min, according to manufacturer's instructions. Cells were washed after staining and air-dried before being viewed under the microscope using the TRITC and DAPI filters. The proliferation and viability of cells cultured on 3D-printed PA-12 in normal and leachate medium were assessed by MTT assay. Briefly, 20 µL of the CellTiter 96® AQueous One Solution Reagent (Promega, USA) was added per 100 µL of the culture medium to each sample and incubated for 4 h at 37°C in a humidified 5% CO_2 incubator before the absorbance was measured at 490 nm in a microplate reader, according with the manufacturer's instructions. MTT assay was performed at the aforementioned timepoints to determine the time-dependent change in cell proliferation and cell number (n = 4 per group).

2.3.3. Surface coating

The surface of 3D-printed PA-12 cell culture chambers and polystyrene 24-well plates was coated with PDL and collagen (CLG) (50 µg/mL) through physical absorption to enhance the attachment of cells on the surface. The PDL- and CLG-coated cell culture chambers were incubated for ~1 h at room temperature following which the chambers were washed thrice with distilled water and PBS, respectively. The above-mentioned coatings were included for all cell culture experiments.

2.3.4. Cell morphology and proliferation

The adherence and growth of cells on 3D-printed PA-12 cell culture chambers were visualized by fluorescence microscopy and SEM by staining the cells with fluorescent dyes (n = 3 per group). For fluorescence microscopy, cells cultured on 3D-printed PA-12 cell culture chambers were fixed, stained, and viewed according to the protocol mentioned in **section 2.3.2**. The viability of cells cultured on 3D-printed PA-12 cell culture chambers was performed at the aforementioned time-points and assessed by MTT assay according to the protocol mentioned in **section 2.3.2**. For SEM, cell culture chambers with cells were fixed with 2.5% glutaraldehyde for 6 h, washed with PBS, and subjected to sequential ethanol series dehydration (50%, 70%, 85%, and 100%) before critical point drying (BALTEC, CPD 030, Critical Point Dryer, Scotia, NY, USA). Samples were then sputter coated and imaged using the protocol mentioned in 2.2.1.

2.3.5. Toxicity analysis

Toxicity analysis was performed by lactate dehydrogenase (LDH) assay at predetermined timepoints using CyQUANT™ LDH Cytotoxicity Assay Kit (Invitrogen, USA) according to manufacturer's instructions. LDH, which was secreted into the supernatant, was determined colorimetrically at OD_{490} using a microplate reader (n = 3 per group).

2.3.6. Intracellular redox status

Cellular glutathione (GSH) level was detected by live-staining cells with a GSH-labeling probe, to detect any oxidative stress induced on the cells by the cell culture chambers sand surface coatings. About 40 µM of monochlorobimane (mBCI) (#M1381MP, Thermofisher, USA) diluted in the culture medium was added to the

cells and incubated for 30 min at room temperature and examined under fluorescence microscope (n = 3 per group). The strength of the fluorescence signal correlates with GSH level and consequently the health of cells.

2.3.7. Proliferation state characterization by immunostaining of Ki67 and p53

To characterize the proliferative state of cells grown on 3D-printed PA-12, the expression of Ki67 (proliferation marker) and p53 (anti-proliferation marker) at protein level were determined by immunostaining. Cells, when fixed and permeabilized, were blocked with 1% BSA in PBS-Tween (0.1%) for 1 h at room temperature and washed before staining. Ki67 was detected with monoclonal anti-Ki67 antibody (#AB16667, Abcam, USA), while p53 was detected with anti-p53 antibody (#AB26, Abcam, USA) according to manufacturer's instruction. Cells were incubated with both antibodies overnight at 4°C. Cells were then washed before incubation with FITC-conjugated goat anti-Mouse IgG (H+L) secondary antibody (Thermofisher, #F2761) and TRITC-conjugated goat anti-Rabbit IgG (H+L) secondary antibody (Thermofisher, #T2769) for 1 h at room temperature and counterstained with Hoechst 33342 (Sigma-Aldrich, #B2261) as described earlier. Cells were then dried at room temperature before viewing under the microscope (n = 3 per group).

2.3.8. Alkaline phosphatase activity

Before differentiation, osteoblasts were seeded at a density of 4000 cells/cm^2 and left in culture to attain confluence. To regulate osteoblast differentiation, osteogenesis induction medium 1 and 2 were used. The osteogenic medium 1 was composed of complete αMEM supplemented with 0.2 mM of ascorbic acid and 10 mM of glycerol 2-phosphate. The osteogenic medium 2 was composed of osteogenic medium 1 with the addition of 50 nM melatonin. When cells were confluent, the normal medium was removed, and osteogenic medium 1 was added. This medium change corresponded to differentiation day 0, and the medium was changed twice a week. On differentiation day 6, osteogenic medium 2 -was added, and the medium was replenished every 3 days. 24 days after differentiation, the alkaline phosphatase (ALP) activity (Alkaline Phosphatase Assay Kit, Abcam, USA) was tested colorimetrically (n = 3 per group). Cells were harvested from cell culture chambers, washed with ×1 PBS, and resuspended in 50 µL of assay buffer. Cells were frozen at −20°C and thawed at 37°C for 5 min to test the ALP activity according to the manufacturer's instructions. Enzyme activity was measured by recording the absorbance at OD_{405}. To determine the number of cells, deoxyribonucleic acid (DNA) was extracted using DNeasy Blood and Tissue Kit (Qiagen, USA), and the DNA content was quantified using Quant-iT™ PicoGreen dsDNA Reagent and Kits (Molecular Probes Inc, USA) by measuring the fluorescence using 480 nm excitation and 520 nm emission. ALP activity was normalized to the total DNA content. The results were expressed in nanomoles of p-nitrophenol produced per microgram of DNA.

2.3.9. Long-term cell culture

In practice, cells are often subcultured for multiple rounds. Accordingly, the effect of growing/subculturing cells on the 3D-printed PA-12 cell culture chambers on the viability and proliferative ability was determined. On reaching confluence (at day 4), cells were subcultured from 3D-printed PA-12 into new PA-12 cell culture chambers and conventional cell culture plates, as indicated in **Figure S1**. As a control, cells were also subcultured from conventional cell culture plates to plates. Two rounds of subculture were performed on day 4 and day 8, for which the cell viability and proliferation were tested on day 8 and day 12, respectively, by MTT assay and fluorescence microscopy, according to the protocol mentioned in **section 2.3.2** (n = 4 per group).

2.3.10. Bacterial adhesion and viability

A. Strains and growth conditions

Escherichia coli strain 0114 (ATCC 25922) was used in this study. Overnight cultures from frozen stock were recovered in 5 mL of brain–heart infusion (BHI) broth and cultured aerobically at 37°C in a shaking incubator. From the overnight culture, an inoculum was prepared in fresh BHI. 300 µL (equivalent to 10^7 bacteria/chamber) of each bacterial suspension was freshly seeded in the 3D-printed PA-12 and positive control (polystyrene plate) cell culture chambers. Both O_2 plasma-treated or untreated PA12 cell culture chambers were tested.

B. MTT assay

The viability of *E. coli* cultured on the 3D-printed PA-12 cell culture chamber was measured using MTT assay (CellTiter 96® AQueous One Solution Cell Proliferation Assay, Promega, USA) to obtain a quantitative value for the absorbance of bacterial units after being cultured for 24 h at 37°C (n = 3 per group). CellTiter 96® AQueous One tetrazolium reagent was added to each well (20 µL/every 100 µL of media) and incubated for 24 h at 37°C. Absorbance was read at 490 nm according to the manufacturer's instructions.

C. Live/dead imaging

The bacterial viability on 3D-printed PA-12 cell culture chambers was observed by staining live bacteria with SYTO9 green and dead bacteria with impermeant propidium iodide (PI) (LIVE/DEAD Bac-Light Bacterial

Viability Kit, Molecular Probes Inc, USA) ($n = 3$ per group). The dyes were mixed at the ratio of 1:1 and used according to the manufacturer's instructions. The excitation/emission wavelength for SYTO9 and PI was 480/500 nm and 490/635 nm, respectively. Randomly selected areas were imaged using a ×20 objective fitted with a fluorescence microscope.

2.4. Statistical analysis

Statistical analysis was performed using the Student's *t*-test, and all the values are expressed as mean ± standard deviation. Differences were considered statistically significant at $P < 0.05$.

3. Results

3.1. Morphological characterization of 3D-printed PA-12 surfaces

First, we compared the microstructure and surface morphology of MJF-printed PA-12 (Figure 1A) and casted PA-12 cell culture chambers (Figure 1B). Representative SEM images of the surface morphology suggested that the 3D-printed PA-12 cell culture chambers display a porous, rough, and irregular microstructure due to partially fused PA-12 powders on the surface (Figure 1C), whereas casted pure PA-12 exhibited a relatively smooth and even texture (Figure 1D). These partially fused powders exhibited a spherical shape with diameters ranging from ~70 to 80 microns (μm). The high-resolution surface images by laser scanning confocal microscopy, shown in Figure 1E and F**,** revealed that the average roughness values (R_a) of 3D-printed PA-12 had a higher surface roughness of ~ 9.4 to 10.4 μm in comparison to pure casted PA-12 (~ 4.3–5.5 μm).

3.2. Surface functionalization with biomolecules

Protein adsorption experiments performed on O_2 plasma-treated and untreated 3D-printed PA-12 cell culture chambers showed that fluorescent signal increases in a dose-dependent manner (Figure 1G) before plateauing at 1% (w/v) (Figure 1H). Moreover, the O_2 plasma-treatment showed little impact on protein adsorption onto the substrate.

The surface energy of 3D-printed PA-12 cell culture chambers assessed by the water contact angle indicated that the uncoated PA-12 cell culture chamber was most hydrophobic with a contact angle of 88.03° ± 3.63°. Surface coating with PDL did not show a significant difference (84° ± 2.62°), whereas the collagen coating significantly reduced the contact angle to 39.4° ± 1.14°, making the surface more hydrophilic. When additional O_2 plasma-treatment was performed after the surface coating, the contact angles of all samples decreased. The contact angle values of uncoated, PDL- and CLG-coated surfaces were 27.5° ± 2.00°, 19.93° ± 1.14° and 21.33° ± 5.42°, respectively.

3.3. Assessment of cell survival on 3D-printed PA-12 surfaces

3.3.1. Effect of leachate medium

L929 fibroblasts and MC3T3e1 osteoblasts cultured in conventional cell culture microwell plate using both normal and leachate medium adhered to the surface and increased in cell density from day 2 to day 4 (Figure 2A, **Figure S2)**. Fluorescence staining showed no signs of abnormality in the cells. When cultured using the leachate medium, cell morphology was preserved and comparable to cells grown in the normal medium. In accordance with these results, the measurements using quantitative MTT assay (Figure 2B and C) indicated that cells grown in the leachate were not affected. Leachate medium did not adversely affect the growth of fibroblasts, whereas osteoblasts survived relatively better ($P < 0.05$) when cultured using the normal medium, but the difference was small (17.67% for day 2 and 11.76% for day 4).

3.3.2. Cell morphology and viability

Short-term culture of L929 fibroblasts and MC3T3e1 osteoblasts in the O_2 plasma-treated, uncoated, and PDL- and CLG-coated cell culture chambers examined by fluorescent staining revealed that cells spread well and exhibited intimate attachment to the surface of 3D-printed PA-12 cell culture chambers on both day 2 and day 4, respectively (Figure 3 and **Figures S3–10**). Conventional polystyrene cell culture plate served as the positive control. The morphology of cells was maintained in all the 3D-printed cell culture chambers, and cells formed confluent layers across the surface topography with an increased cell density observed on day 4. In the background, stained globular surface structures showed the roughness of MJF-printed PA-12. This corroborated with the electron micrographs in Figure 1C, 4A and B. Nevertheless, the background signal did not affect the visualization of cells. Rather, the stained background illuminated the topological context, in which the cells were attached and grew in the printed PA-12 chamber, providing us with more insight on how the cells would appear on the printed surface. Cells can still be clearly observed, especially in areas, where there was weaker non-specific noise. Representative results of cells cultured on PDL-coated cell culture chambers are shown in Figure 3A. It can be observed that cells, when grown on the 3D-printed PA-12 surface, exhibited strong actin cytoskeleton architectures and prominent nuclei.

MTT studies determined the level of cell proliferation (Figure 3B and C). The signal increased

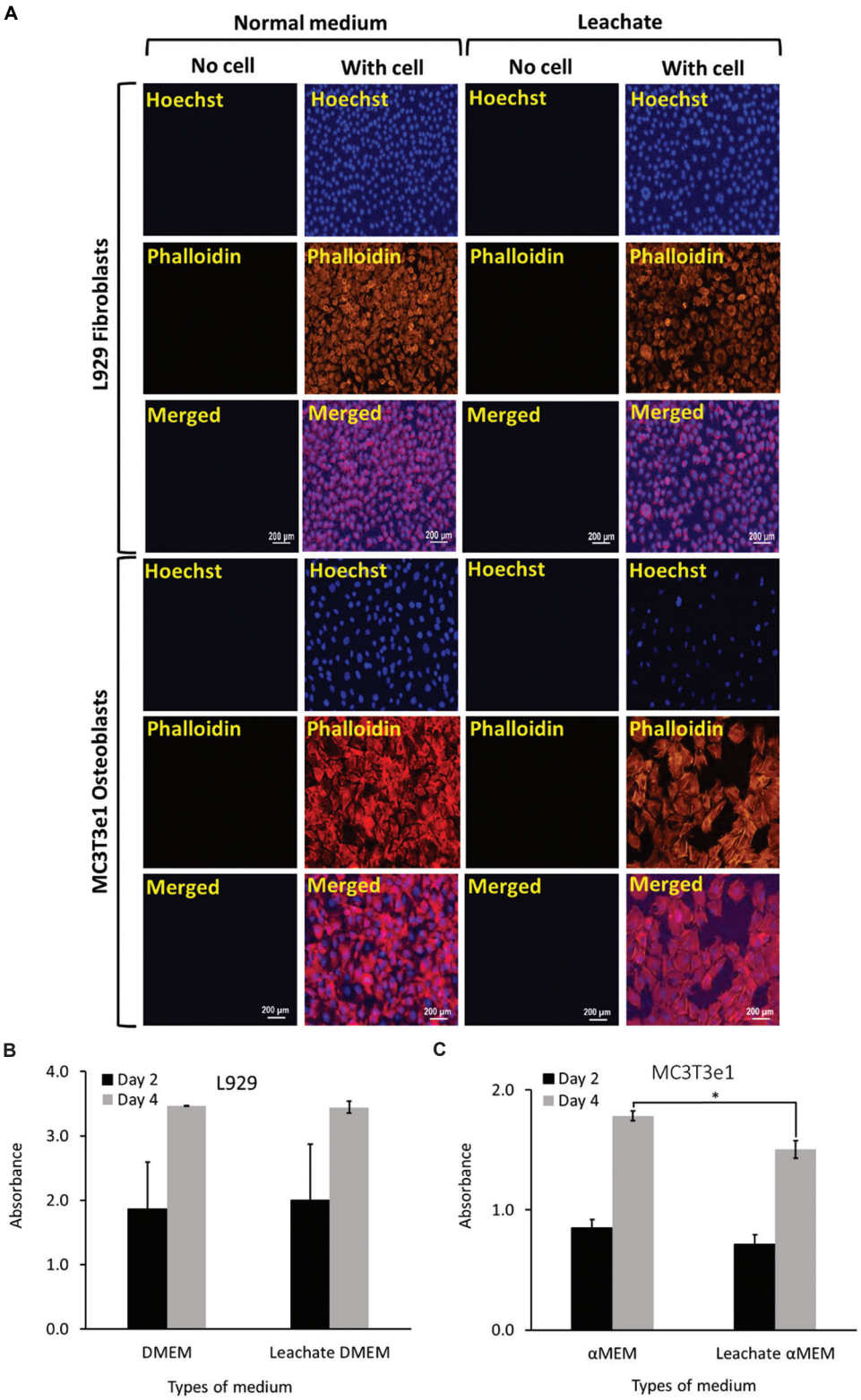

Figure 2. (A) Representative fluorescence microscopy images of L929 fibroblasts and MC3T3e1 osteoblasts cultured using normal and respective leachate medium showing cell growth and increase in cell density following culture on cell culture chambers (plates) on day 4. A graph of MTT assay showing the viability of (B) L929 fibroblasts and (C) MC3T3e1 osteoblasts cultured using the respective leachate medium after day 2 and day 4, respectively.

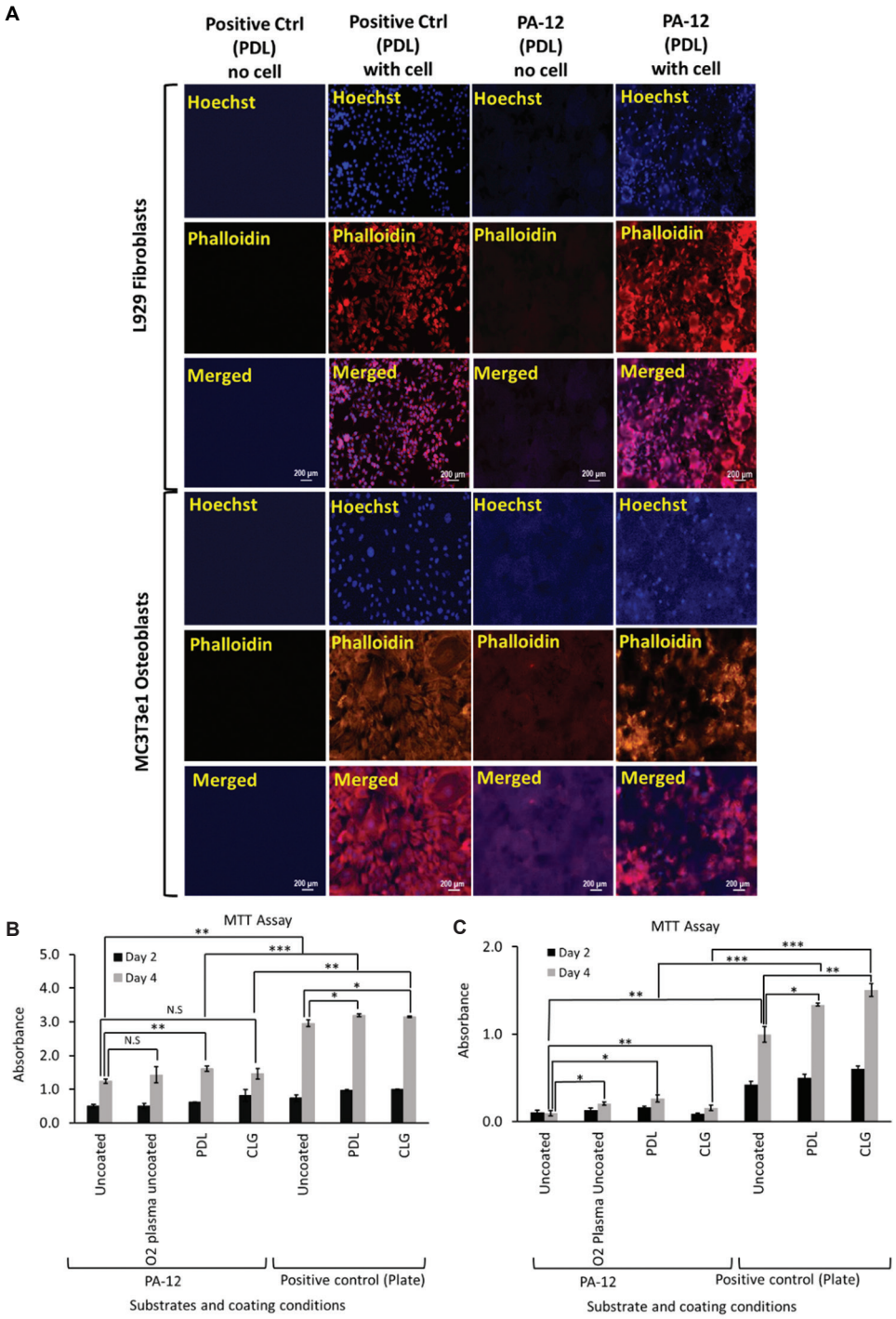

Figure 3. (A) Representative fluorescence microscopy images of L929 fibroblasts and MC3T3e1 osteoblasts cultured on PDL-coated 3D-printed PA-12 and positive control (plate) cell culture chambers after 4 days. A graph of MTT assay showing viability of (B) L929 fibroblasts and (C) MC3T3e1 osteoblasts cultured on uncoated, O_2 plasma-treated, PDL- and CLG-coated 3D-printed PA-12, and positive control (plate) cell culture chambers after day 2 and day 4, respectively. * ($P < 0.05$), ** ($P < 0.01$) and *** ($P < 0.001$) denote statistical significance. N.S, Not significant.

in a time-dependent manner, indicating that both cell types proliferated from day 2 to day 4. However, higher signal was observed on polystyrene plate in comparison to that in 3D-printed PA-12 chambers. L929 fibroblasts proliferated better ($P < 0.05$) on both PDL-coated polystyrene and 3D-printed PA-12 surfaces relative to

those on the uncoated surface in comparison to other coating or plasma-treatment, as determined at day 4 timepoint. On the other hand, MC3T3e1 osteoblasts grew better on PDL-coated 3D-printed PA-12 ($P < 0.05$) and CLG-coated polystyrene plate ($P < 0.05$). These observations indicated that PDL was the preferred choice as an extracellular matrix for culturing cells of both types on 3D-printed PA-12, even though it did not substantially narrow the gap with polystyrene plate. The fact that fibroblasts survived better in the 3D-printed PA-12 cell culture chambers than osteoblasts during short-term culture was apparent. Cells demonstrated equal proliferation on uncoated hydrophobic PA-12 surfaces, even in the absence of surface coating or O_2 plasma-treatment, indicating that the surface wettability did not significantly affect the cell adherence. When substrates were plasma-treated, a significant decrease in hydrophobicity was observed ($P < 0.05$). Even though substrates demonstrated higher wettability, this did not significantly improve the cell adhesion on the substrates. Therefore, hydrophobicity was not considered a key factor in determining the biocompatibility of 3D-printed PA-12.

Representative SEM images of L929 and MC3T3e1 cells cultured on 3D-printed PA-12 and polystyrene cell culture chambers are shown in Figure 4A–D. In all the experiments, L929 fibroblasts and MC3T3e1 osteoblasts cultured on coated and uncoated 3D-printed PA-12 cell culture chambers presented a flat morphology and appeared intimately adherent to the surface, with no specific orientation. L929 fibroblasts and MC3T3e1 osteoblasts cultured on coated and uncoated 3D-printed PA-12 cell culture chambers appeared intimately adherent to the surface and showed an increase in the number of cells attached to the surface, noticeable after 4 days of incubation. Fibroblasts exhibited cellular dimensions (~15 µm in diameter) (Figure 4A i–iii) smaller than the unfused PA-12 particles, making it conducive for cells to adhere to a single particle. Interestingly, unlike in the fluorescent images, the morphology of L929 grown on PA-12 and polystyrene appeared different in the SEM images. Such differences could be devoted to intrinsic artifacts such as specimen shrinkage[55] more likely as an effect of glyceraldehyde fixation[56] or ethanol dehydration[57] before critical point drying. Some earlier studies had also suggested great variation of these artifacts from one type of sample to another[58]. It was also indicated that the use of high-resolution SEM had known to accentuate artifacts which might otherwise appear minimal at a lower resolution[59]. In addition, the influence of the MJF-printed PA-12's surface properties (such as roughness) on preserving cell appearance from the effect of SEM-processing methods had to be highlighted. Moreover, the literature had minimal evidence on the effect of critical point drying on 3D-printed PA-12, which had a major role in deciding on how the cells appeared and survived on seeding. Nonetheless, the electron micrographs provided additional evidence showing the presence and adherence of cells on the printed PA-12. In contrast, a completely different behavior was observed for osteoblasts which were bigger in size (>50 µm) compared to fibroblasts. Osteoblasts exhibited a flattened shape and appeared to spread over multiple particles and had many prominent filopodia protrusions stretching over multiple particles (Figure 4B i–iii). As a result, the main cell body appeared loosely attached and suspended between particles, making it difficult for the osteoblasts to completely attach and proliferate. Control PA-12 cell culture chambers (medium only) are also shown for reference (**Figure S11A i–iii** and **S11B i–iii**). Fibroblast and osteoblasts cells (and control samples without cells) grown on polystyrene cell culture chambers are also shown for comparison (**Figure S11C i–iii** and **S11D i–iii**). Taken together, these findings supported the fact that 3D-printed PA-12 can support cell growth, but not to the extent observed on polystyrene plates, probably due to the microroughness resulting from partially fused particles on the surface among other factors.

3.3.3. Cellular toxicity

The short-term exposure of L929 fibroblasts and MC3T3e1 osteoblasts to uncoated, PDL- and CLG-coated 3D-printed PA-12 cell culture chambers, and polystyrene plate resulted in minimal LDH secretion due to cellular membrane integrity on day 2 and day 4, respectively. Consequently, cells cultured on both coated (PDL and CLG) and uncoated 3D-printed PA-12 demonstrated no signs of cytotoxicity. No significant difference in cytotoxicity was observed between coated and uncoated substrates, as shown in Figure 5A and B.

3.3.4. Redox characterization

Visualization of oxidative stress assessed by mBCI staining of L929 fibroblasts and MC3T3e1 osteoblasts cultured on 3D-printed PA-12 cell culture chambers and polystyrene plate showed preservation of intracellular reduced GSH on both day 2 and day 4, regardless of the type of surface coating (uncoated and coated) (Figure 5C and **Figure S12**). For fibroblasts, GSH-mBCl fluorescence signal was comparable between cells grown on 3D-printed PA-12 cell culture chambers and polystyrene plates at both time points, suggesting that cells were not significantly stressed on culture in 3D-printed PA-12 cell culture chambers. However, osteoblasts cultured on 3D-printed PA-12 showed a reduction in the overall intensity when compared to that observed on polystyrene plate, possibly as a result of the lower cell count.

3.3.5. Cellular proliferation

The proliferative state of cells characterized by immunostaining of Ki67 and p53 suggested that

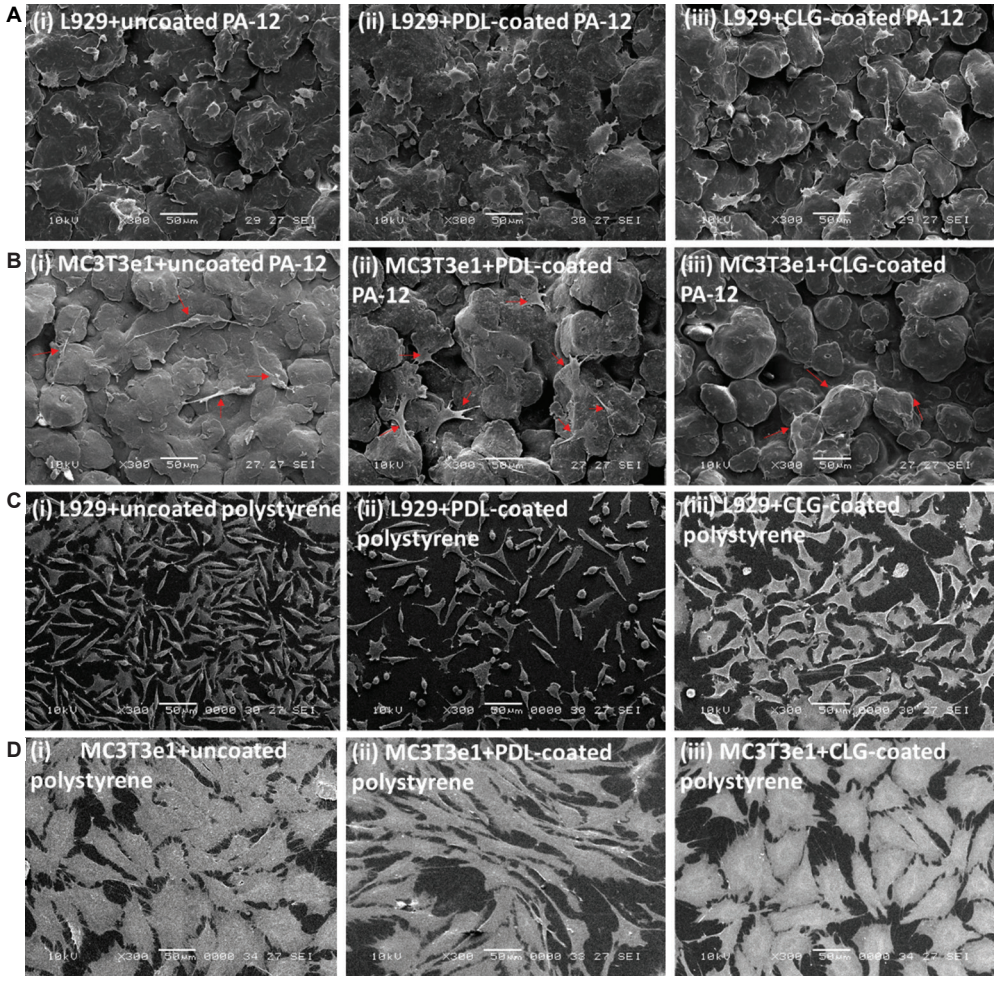

Figure 4. Representative scanning electron microscopy images showing the morphology of (A) L929 fibroblasts and (B) MC3T3e1 osteoblasts cells cultured on (i) uncoated, (ii) PDL-coated, and (iii) CLG-coated 3D-printed PA-12 cell culture chambers after 4 days of culture. The red arrows are used to specify the location of the cells. Representative scanning electron microscopy images showing the morphology of (C) L929 fibroblasts and (D) MC3T3e1 osteoblasts cells cultured on (i) uncoated, (ii) PDL-coated, and (iii) CLG-coated polystyrene cell culture chambers after 4 days of culture.

the expression pattern observed in cells cultured on 3D-printed PA-12 cell culture chambers was similar to that grown on the positive control (polystyrene plates) on day 2 and day 4, respectively (Figure 6A). It was observed that only Ki67 is expressed and markedly upregulated in cells cultured in all cell culture chambers, whereas p53 was downregulated (**Figures S13**–**S18**). Stronger fluorescent signals were observed in fibroblasts in comparison to osteoblasts. This result suggested that 3D-printed PA-12 cell culture chambers did not alter the gene expression of Ki67 and p53.

3.3.6. ALP activity

ALP activity of differentiated MC3T3e1 osteoblasts cultured in 3D-printed PA-12 cell culture chambers is shown in Figure 6B. The ALP activity on positive control plates (coated and uncoated) before normalization are shown in **Figure S19**. On day 28, cells cultivated in the differentiation medium expressed higher levels of ALP ($P < 0.05$) than the undifferentiated one, indicating that cells were capable of differentiation on 3D-printed PA-12. This suggested that cells cultivated on PA-12 were capable of differentiation.

3.3.7. Long-term serial passaging

To demonstrate the proliferative ability, cells were subcultured from 3D-printed PA-12 into new PA-12 cell culture chambers and conventional cell culture plates, respectively, according to the experimental scheme, as shown in **Figure S1**. Prolonged culture of cells did not negatively impact the cell adherence nor affected long-term serial passaging, as shown in Figure 7A.

Cells after the first and second passages also adhered and attached to the PA-12 cell culture chambers without any sign

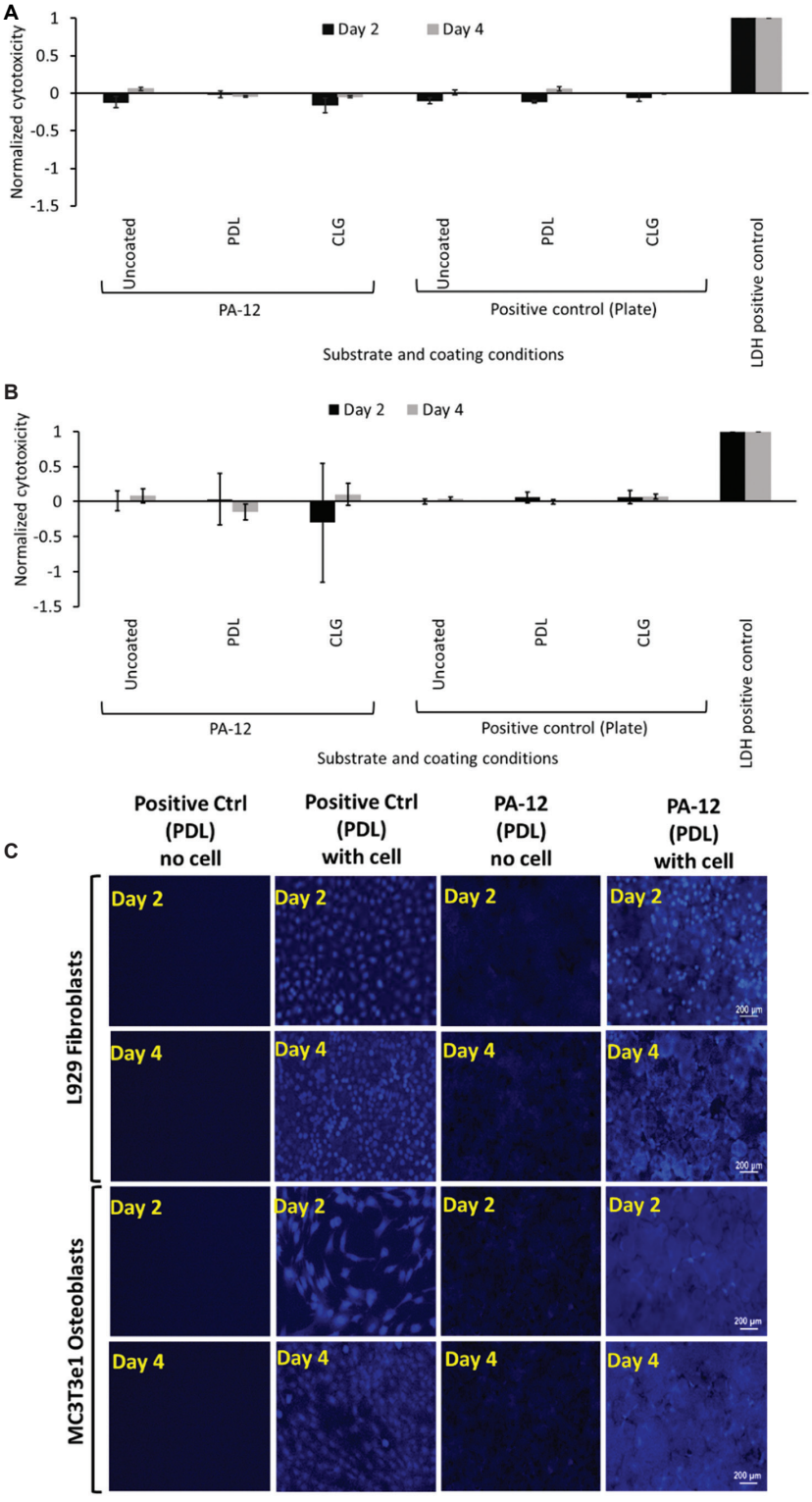

Figure 5. Graph of LDH release from (A) L929 fibroblasts and (B) MC3T3e1 osteoblasts cultured on uncoated, O_2 plasma-treated, PDL- and CLG-coated 3D-printed PA-12, and positive control (plate) cell culture chambers after day 2 and day 4, respectively. LDH released from each sample was normalized with endogenous LDH released by lysis to obtain the normalized cytotoxicity. A positive control of pure LDH was included as a reference with a value fixed at 1. (C) Representative fluorescence microscopy images of L929 fibroblasts and MC3T3e1 osteoblasts stained for glutathione evaluation following culture on PDL-coated 3D-printed PA-12 and positive control (plate) cell culture chambers after day 2 and day 4, respectively.

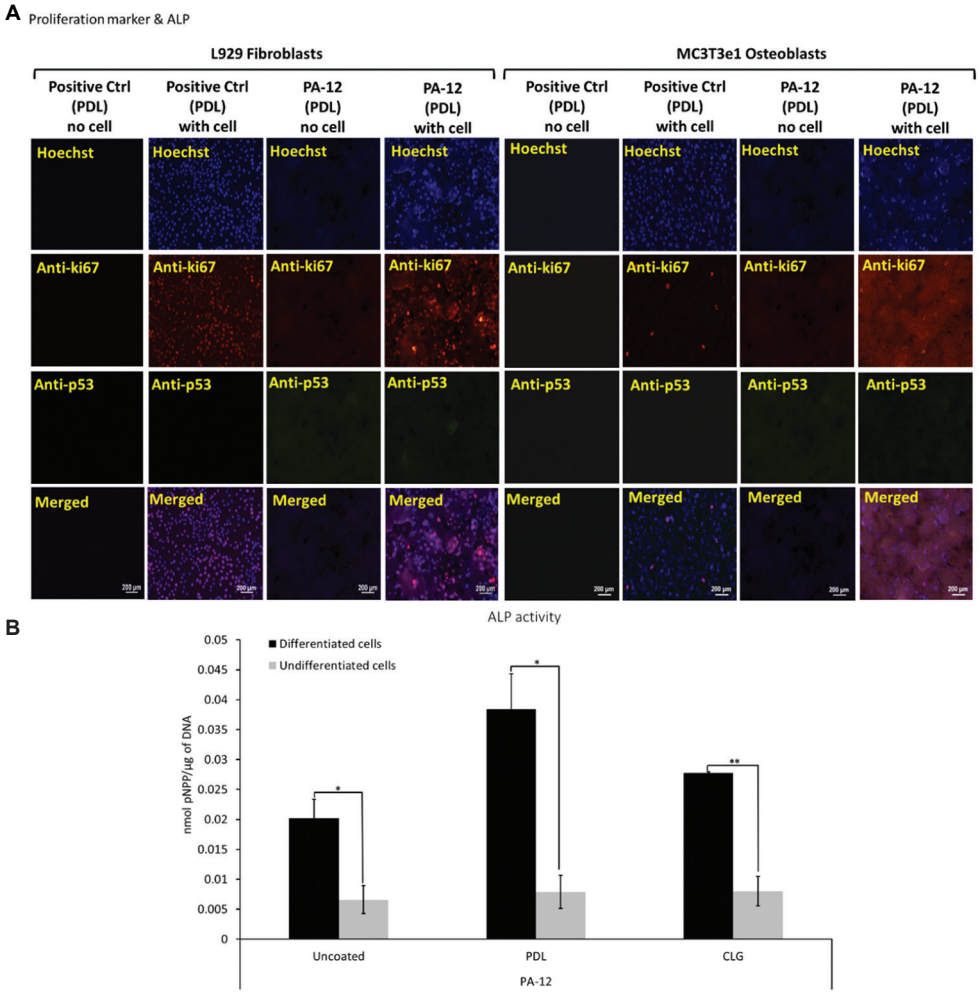

Figure 6. (A) Representative fluorescence microscopy images of L929 fibroblasts and MC3T3e1 osteoblasts immunostained to determine the expression of ki67 and p53 following culture on PDL-coated 3D-printed PA-12 and positive control (plate) cell culture chambers after 4 days. (B) Alkaline phosphatase activity (normalized) of MC3T3e1 cultured on uncoated, PDL- and CLG-coated 3D-printed PA-12 cell culture chambers at day 28.

of abnormality or changes in cell appearance, comparable to that observed on polystyrene plate (**Figures S20–S25**). The fibroblasts continued to grow robustly and proliferated well when subcultured from PA-12 to PA-12 as well as from PA-12 to the polystyrene control plate as confirmed by the MTT assay (Figure 7B and C). As observed in the short-term culture, fibroblasts grew better in comparison to osteoblasts. After first passage, osteoblasts adhered to PA-12 cell culture chambers; however, a reduction in their proliferation was represented by the decreased MTT signals which can be noted even in positive control at day 12. After second passage, significant exhaustion of the MC3T3e1 proliferative capacity was observed (Figure 7C).

3.3.8. Bacterial viability and fouling

Examination of 3D-printed PA-12 cell culture chambers showed heavy and dense growth of bacteria (green) uniformly covering the entire surface after 24 h, as shown in Figure 8A. The bacterial viability on 3D-printed PA-12 cell culture chambers was comparable to that observed on conventional culture plates (positive control), suggesting strong bacterial attachment. The big green spheres in the background were due to the non-specific staining of the partially fused PA-12 particles. The contribution of red fluorescence, which represented the dead bacteria, was less predominant, indicating that the fraction of dead bacteria was significantly lower. The viability experiments by MTT assay further supported these results. Adhered bacteria on the surface of PA-12 cell culture chambers (after 24 h), when tested directly for viability, indicated good bacterial activity (Figure 8B). No inhibiting effect of PA-12 on the growth, fouling, and viability of the bacterial cells was observed.

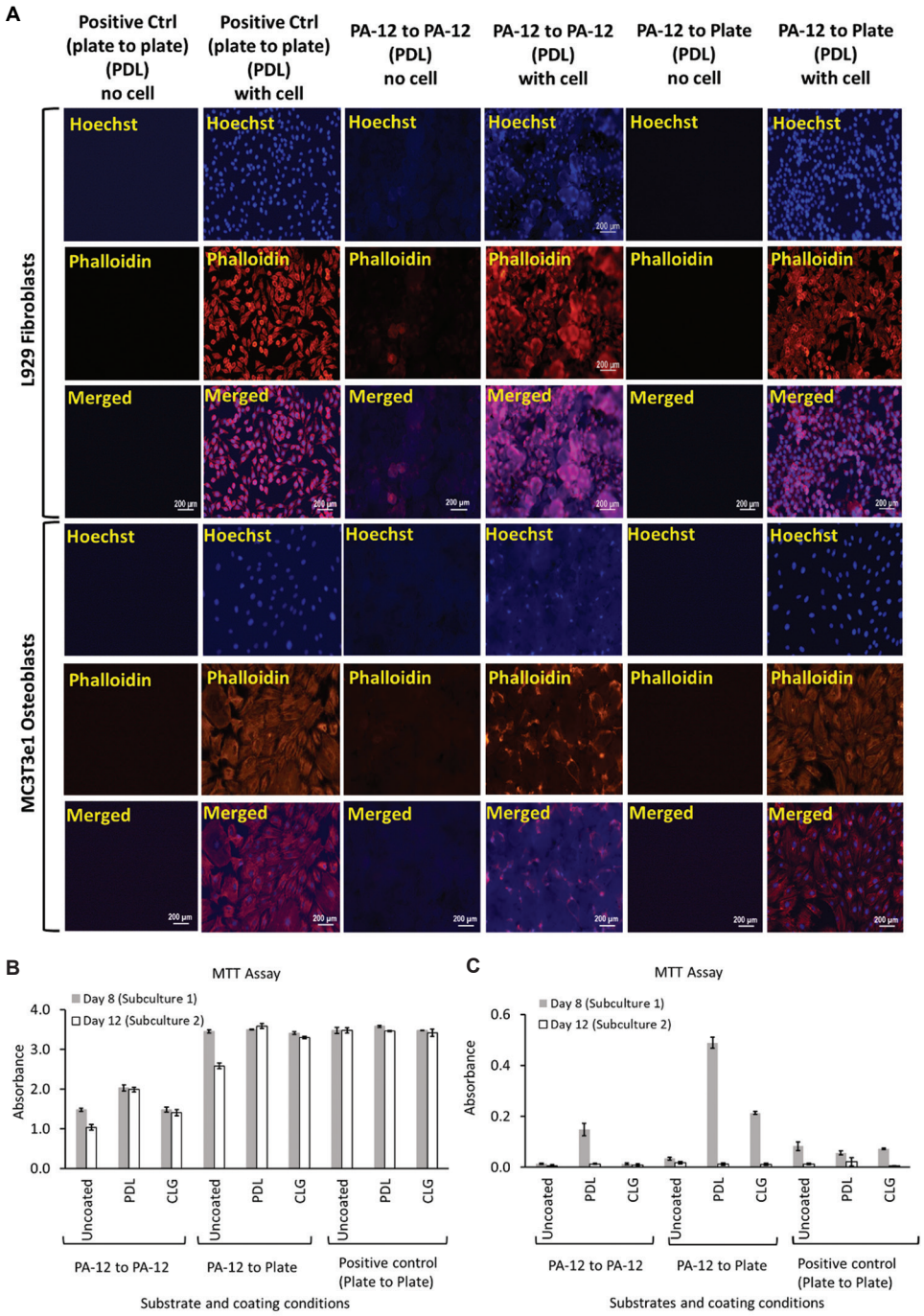

Figure 7. (A) Representative fluorescence images of L929 fibroblasts and MC3T3e1 osteoblasts cultured on PDL-coated 3D-printed PA-12 and positive control (plate) cell culture chambers following long-term culture after 12 days. A graph of MTT assay showing viability of (B) L929 fibroblasts and (C) MC3T3e1 osteoblasts following long-term subculture on uncoated, O_2 plasma-treated, PDL- and CLG-coated 3D-printed PA-12 and positive control (plate) cell culture chambers after day 8 and day 12, respectively.

4. Discussion

The choice of the right 3D printing technology and material is vital for the fabrication of bioreactors. MJF is a relatively new polymer-based PBF method introduced by HP that frequently uses PA-12 as the prime powder material. The novelty of this work is based on the fact that the PA-12 cell culture substrates were printed by an in-house MJF 3D printer. However, it is important to note that this technology uses fusing and detailing agents to deliver

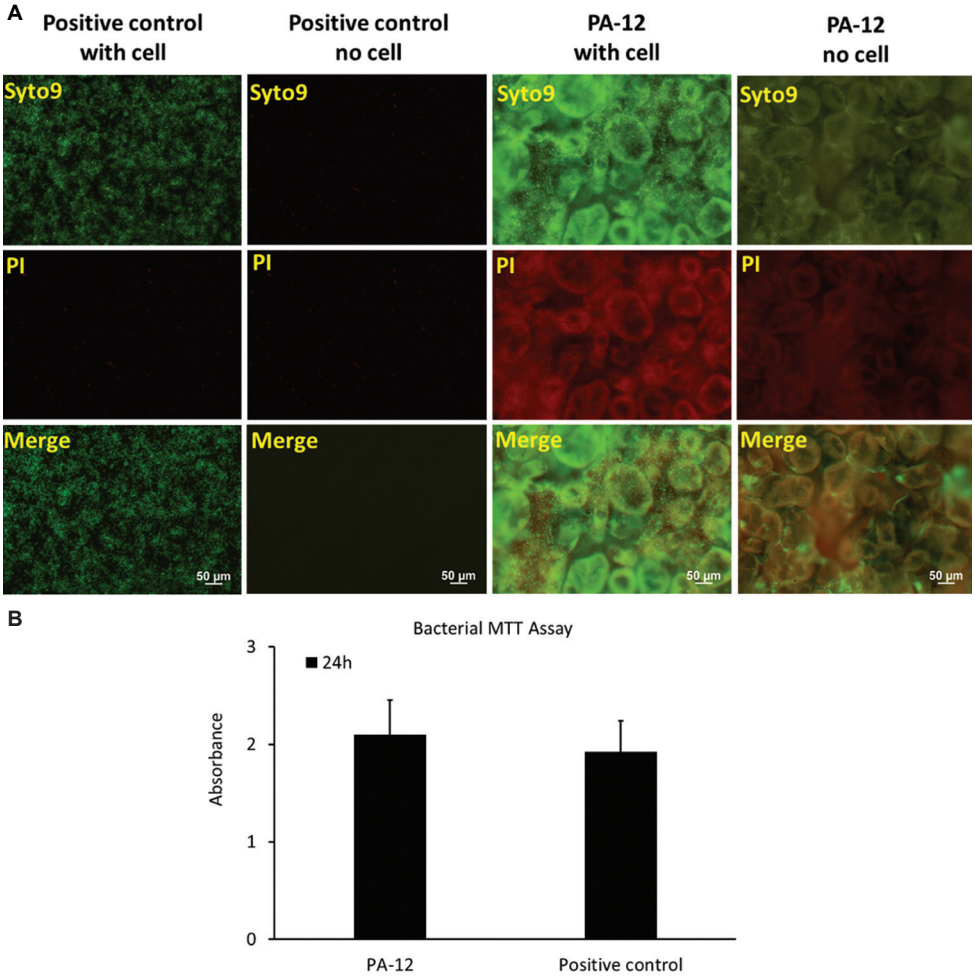

Figure 8. (A) *Escherichia coli* cultivated on 3D-printed PA-12 and positive control (plate) cell culture chambers and visualized with fluorescence microscopy using BacLight LIVE/DEAD stain, which stained live cells green and compromised (dead) cells red. (B) MTT assay showing viability of *E. coli* cultured on 3D-printed PA-12 and positive control (plate) cell culture chambers after 24 h.

quality, functional parts[54]. Accordingly, the effect of the presence of these components on the biocompatibility of printed parts remains to be identified. So far, this is the first study that focuses on the use of MJF-printed substrates for life science applications. This study opened the door for use of 3D-printed PA-12 as a bioreactor. Furthermore, the cells that were used in this study were mostly robust cell lines which will likely grow on most surfaces. However, we specifically tested the ability of cells to adhere and proliferate on these MJF-printed substrates.

In addition to its ability to print parts that are stronger and more precise, MJF demonstrates a faster printing process/production speed in comparison to SLS with high-quality printed parts and high-throughput printing[60]. Since this process uses a powder-based material, the finished products are susceptible to defects such as rough surface, lack of fusion, and porosity[61]. Even with the inclusion of detailing agent, morphologies with rough and uneven surface texture are observed due to coarse spherulites contained in reclaimed and reused PA-12 powder (Figure 1C and E), following post-crystallization and spherulite growth[62,63]. Moreover, the partially fused PA-12 powder particles would detach from the surface, leaving voids and making the surface porous (Figure 1C), which is considered as a design limitation.

The material surface and topography are crucial in improving and controlling the cellular response. Modification of the surface chemistry directly influences protein adsorption and therefore cell behaviors. By altering functional groups present at the material surface, it is possible to tailor its surface properties, and consequently its wettability, cell adhesion, and proliferation[7]. As part of the material surface optimization, 3D-printed PA-12 surfaces are functionalized by O_2 plasma activation and tested for

protein binding capability using BSA-FITC. Earlier studies demonstrate the use of low-pressure O_2 plasma to activate porous surfaces for significantly increasing the utility value of 3D-printed products by improving previously inaccessible poor surface properties of the products[64]. The protein adsorption experiments using BSA-FITC indicated successful dose-dependent protein capture that plateaus, suggesting saturation, at around 1%, indicating a possibility that the surfaces of 3D-printed materials can simulate the properties of natural extracellular matrix aiming to regulate the behavior of cell adhesion (Table 1). This may also suggest that the spatial conformation of the adsorbed biomolecules plays a key factor in mediating cell adhesion rather than the concentration or amount of molecules affecting the adhesion process[65]. However, there is no significant difference between O_2 plasma-treated and untreated cell culture chambers (Figure 1G and H). In this case, however, O_2 plasma-treatment does not enhance the protein binding capability of MJF-printed PA12[61]. Based on this observation, 3D-printed PA-12 are directly functionalized with biopolymers such as PDL and CLG (at 50 μg/mL), commonly used biomolecules that help in initiating cell attachment and maintaining cell growth.

The primary focus of this work is to evaluate the biocompatibility of 3D-printed PA-12 cell culture chambers. The choice of assays plays a key role in assessing the material cytotoxicity, while other parameters, such as controls, cell lines, period of culture, and other biochemical events are crucial in testing a material's compatibility[66]. Here, we study the biocompatibility of 3D-printed PA-12 by 2 methods: (i) by indirectly exposing the cells to the leachate medium that is extracted by exposing the culture medium to 3D-printed PA-12 parts and (ii) by directly seeding the cells on the surface of the material (short- and long-term culture). This study, which employs multiple cell lines, including L929 fibroblasts and MC3T3e1 osteoblasts grown on surface-coated 3D-printed PA-12, shows a significant difference in their sensitivity toward the cell culture chambers.

Both fibroblast and osteoblast cells show the ability to grow in the leachate medium (Figure 2A and Figure S2). Fibroblasts grow well regardless of whether it is cultivated in the leachate or the normal medium. However, osteoblasts grown in the leachate demonstrate a drop in the MTT values at day 4 compared to those grown in αMEM, suggesting that they proliferate better in the normal medium in comparison to the leachate (Figure 2B and 2C). Although it is statistically different, the difference is small. As aforementioned, the leachate medium is prepared by soaking PA-12 cell culture chambers in the respective cell culture media. Small molecules that leach into the medium, possibly from fusing and detailing agents, may have caused this effect, as indicated in Table 1. Therefore, the growth of a certain cell type is slower in leachate compared to the control. Otherwise, no other potential material leaching issue is observed in our experiments as the typical test only uses leachate medium exposed to MJF-printed PA-12 for 5 days. Further, investigations are underway to unravel the effect of material leaching with regards to cell growth. However, further studies are required to probe into cell line specific *in vitro* toxicity and cytocompatibility of 3D-printed PA-12.

As shown in MTT studies from direct culture in 3D-printed PA-12 cell culture chambers, L929 fibroblasts adapt well and proliferate efficiently when cultured in the 3D-printed PA-12 (Figure 3B and 7B) cell culture chambers, whereas osteoblasts did grow and proliferate, but to a lesser degree (Figure 3C and 7C). The observed reduction in proliferation of osteoblasts could be related to the fact that MTT activity is directly proportional to the cell number[67]. Moreover, osteoblasts appear larger in size compared to fibroblasts, as shown in Figure 3A and **Figures S3–S10**. Many osteoblast cells (Figure 4B) are suspended between two particles, whereas fibroblasts fully attach on one particle. SEM images after 4 days of culture show that the L929 cells are more or less rounded in shape, orientate symmetrically with small cellular extensions aiding in

Table 1. A summary of key MJF-printed PA-12 features of interest, their associated problems, and our results addressing them in this study

Printed substrate's features	Potential problems	Results
PA-12's binding affinity for protein biomolecules	• Ease of surface functionalization with extracellular matrix	• Printed PA-12 can bind to BSA, indicating surface modification with protein extracellular matrix is possible
Surface topography/roughness	• Impaired cell adhesion • Abnormal cell morphology	• Cells can adhere to printed PA-12 from passage to passage • While fluorescence microscopy does not indicate an obvious change in cell morphology, SEM shows fibroblast displaying unusual morphology
Fusing and detailing agents	• Cytotoxicity • Growth inhibition • Differentiation inhibition	• No cytotoxicity is detected • Cells can proliferate, though not as good as on polystyrene surface • Osteoblast can differentiate

high cell assembly on PA-12 particles (Figure 4A). On the other hand, osteoblasts are mostly irregularly flattened with elongated filopodia extensions roughly equally from each side of the cell that appears extensively spread. The uneven PA-12 surface and the large size of osteoblasts cause the cells to stretch/extend over many unfused particles. This facilitates the attachment of the filopodia extensions causing a "pulling effect" on the cell edges, and therefore, the main cell body appears unattached and suspended from the PA-12 substrate (Table 1). Moreover, the rougher PA-12 surface makes it difficult for osteoblast to reach confluence. Hence, a stable surface attachment evidenced in fibroblasts is not seen in osteoblasts, making it difficult for them to proliferate in the same way. In contrast, cells grown on polystyrene substrates are well adherent, proliferative and particularly attain confluence (Figure 4D i–iii). However, cell morphology with spread and expanded cytoskeleton remained similar to that observed on PA-12. The osteoblast morphology, proliferation, and metabolic activity seem to be more sensitive to the topography of the substrate. The results suggest that the surface roughness of MJF-printed 12 has a differential effect on the proliferation of different cell types. It negatively affects MC3T3e1 more than L929, possibly due to the larger cell size of the former. Since adhesion is a necessary step in promoting cell growth, the imperfect contacts between MC3T3e1 and the surface could have weakened the transduction of growth signaling pathway from the extracellular matrix to the cells. This can be addressed by polishing the surface of printed PA-12 with sandpaper to smoothen out all the irregular globular bumps. Alternatively, the surface could be coated with a layer of biocompatible polymer, such as polystyrene, to form a smooth even surface for attachment. Smoothening the surface is expected to enhance not just MC3T3e1 but also L929, attachment, and proliferation. To further characterize the effect of roughness on cell growth, a combination of other evaluation assays is included to further test the *in vitro* cytotoxicity.

The LDH assay is another commonly used marker for cell death. Negligible LDH release is observed in both cell lines (Figure 5A and 5B), indicating no cell death nor cell membrane damage as the cells continue to proliferate after day 4 (as suggested by long-term culture studies, Figure 7A–C and Figures S20–S25). Moreover, the influence of oxidative stress in causing cytotoxicity is correlated to the upregulation or downregulation of various gene regulatory proteins. Since the intracellular GSH levels are significantly higher (as represented by high mBCI fluorescence signals in Figure 5C and Figure S12), corresponding levels of proliferative marker (Ki-67) are observed at day 2 and day 4 (Figure 6A). The absence of p53 antigen (anti-proliferative marker) in both cases suggests cells cultured on 3D-printed PA-12 cell culture chambers that are actively proliferating cells and remain unaffected. The expression of the nuclear Ki-67 antigen is strictly associated with cell proliferation and not present in resting or quiescent cells, in which many proliferation-related proteins remain degraded[68]. As a useful predictor for recognizing rapidly proliferating cells, Ki-67 is constitutively expressed by fibroblasts (**Figures S13–S15**). However, studies indicate that it may also be present in low levels in some cells (like osteoblasts as observed in **Figures S16–S18**)[69].

During *in vitro* cell culture, long-term successive cell passaging is inevitable. Even though the osteoblast adherence and morphology are sustained in prolonged cultures (Figure 7A), the viability and proliferation ability are greatly compromised in MC3T3e1 osteoblasts after continuous passaging (Figure 7C). While culturing MC3T3e1 osteoblasts, the passage number of the cells matter as they can influence cell function. Cells at passage 25 are used for this study. Researchers advise against the use of osteoblast cells above 30 passages which involve few risks that occur beyond safe passage[70]. Moreover, cells are revived from a -80°C freezer during which the cell physiological activities are maintained at a relatively lower level. It might take a couple of passages for the cells to recover in terms of functionality[71]. It is no surprise that the osteoblasts are less functional given their retarded proliferative behavior under normal circumstances when cultured on 3D-printed PA-12 cell culture chambers as aforementioned. The same phenomenon is also observed in positive controls (Figure 7C). When using osteoblast cells, such complications during culture may arise when considering interspecies differences, primary versus established cell cultures, and the possibility of phenotypic heterogeneity of osteoblastic cells when obtained from different anatomical sites[72].

Unlike MC3T3e1, there is no evidence in our results suggesting that PA-12 impaired the L929 fibroblast's ability to proliferate from subculture to subculture. However, certain morphological abnormalities were also observed mostly due to the surface topography of different substrates indicating the fact that even though cells adhere to the substrates, they may not have completely adapted to the topography of its surface (Table 1). Of note, cells transferred from PA-12 to plate retain the ability to grow as robustly as those subcultured from plate to plate. PA-12, especially the coated ones, did not impair their ability to grow on conventional culture plates in subsequent subculture (Figure 7B). This is important firstly because we do not want PA-12 to affect cells ability to grow on other surfaces. Certain practical applications may necessitate cells to be subcultured from one type of substrate to another. Second,

these results suggest that the less robust growth of cells on PA-12 observed previously in our MTT assay for short-term culture (Figure 3B) is not due to any permanent damage to the cells. This is consistent with our Ki-67/p53 expression (Figure 6A and Figures S13–S18) and oxidative stress (Figure 5C and Figure S12) results which suggest no obvious sign of change in the proliferation profile and redox status of cells grown on PA-12. Moreover, 3D-printed PA-12 in the presence or absence of aforementioned surface coatings demonstrates the capability to enhance osteogenesis in MC3T3e1 osteoblasts, which indicates surface coatings as a potential regulator in osteoblast differentiation (Figure 6B). Even though direct culture with the leachate medium indicated growth inhibition to some extent possibly due to the interference from fusing and detailing agents, the ability of osteoblasts to differentiate has not been compensated, as suggested in Table 1. Taken together, while cells are able to grow, proliferate, and differentiate on MJF-printed PA-12, the substrate supports the long-term growth of certain cell types better than the other.

Microbial growth and fouling in 3D-printed PA-12 reaction chamber emphasizes the fact that this material does not show any anti-fouling and antimicrobial capabilities. Previously, studies that focus on the bacterial attachment to polymer surfaces use *E. coli* as a model organism[73]. A closer look at the fluorescent images taken after 24 h of incubation suggests that PA-12 surfaces are as effective as polystyrene at retaining bacterial cells on the surface, as shown in Figure 8A. Majority of the cells remain viable throughout the duration of the experiments. In accordance with these findings, the MTT results further confirm the bacterial growth and viability from early bacterial colonization of PA-12 surfaces (Figure 8B), a critical stage during which cell-material interactions occur to yield a sustainable population. These findings are consistent with the fact that a rough surface with R_a larger than the dimension of *E. coli* (~1 – 2 μm × 0.5 μm) retains bacteria on the surfaces, probably due to an increase in surface area for adhesion[74]. However, long-term investigations have to be conducted to monitor the bacterial attachment and possible biofilm fouling beyond the 24 h timepoint.

5. Conclusion

MJF technology has shown exciting potentialities due to its design flexibility, faster overall production cycle than other 3D printing techniques, and strategy to minimize waste by employing recyclable and reusable powders. One potential application, where such benefits can be exploited, is in the fabrication of bioreactors. While 3D printing has already found its way into bioreactor applications, the use of different processes and materials in the novel MJF technology necessitates a thorough evaluation of the biocompatibility of such products. For MJF-printed materials to be used as a bioreactor, it must be able to support not just cell growth and proliferation, but also other complex and highly regulated processes such as osteogenesis. This study presents an examination of 3D-printed PA-12 with regard to material surface property and biocompatibility. Our results indicate that the MJF-printed PA-12 can be considered appropriate for use as a customized cell culture chamber/vessel due to its non-cytotoxic properties. However, MJF-printed bioreactors exhibit varying ability in supporting different cell types and biological processes. Such disparities between the MJF-printed substrate and polystyrene plate could be attributed to the different responses of distinct cell types to possible influences by surface topography resulting from the microcavities and concave globular microstructures on the uneven surface. Our study provides findings on how well different cell types grow on PA-12 printed by MJF technology, thus contributing to the continuing development of PBF 3D printing for biomedical application. Given the benefits of MJF technology and the outstanding properties of PA-12, we believe that this study has laid the groundwork for a more comprehensive characterization in the future development of MJF-printed PA-12 to realize its eventual commercial use in biological application.

Acknowledgments

None.

Funding

This research was conducted in collaboration with HP Inc. and supported/partially supported by the Singapore Government through the Industry Alignment Fund-Industry Collaboration Projects Grant.

Conflict of interest

The authors declare no conflicts of interest.

Author contributions

Conceptualization: Yi Zhang
Formal analysis: Balasankar Meera Priyadarshini, Wai Kay Kok
Funding acquisition: King Ho Holden Li, Yi Zhang
Investigation: Balasankar Meera Priyadarshini, Wai Kay Kok, Vishwesh Dikshit, Shilun Feng
Writing – original draft: Balasankar Meera Priyadarshini, Wai Kay Kok, Vishwesh Dikshit
Writing – review & editing: Balasankar Meera Priyadarshini, Wai Kay Kok, Vishwesh Dikshit, King Ho Holden Li, Yi Zhang

Ethics approval and consent to participate

Not applicable.

Consent for publication

Not applicable.

Availability of data

All data are presented in the manuscript and the Supplementary File.

References

1. Shahrubudin N, Lee TC, Ramlan R, 2019, An overview on 3D printing technology: Technological, materials, and applications. *Proc Manuf*, 35: 1286–1296.
2. Buchanan C, Gardner L, 2019, Metal 3D printing in construction: A review of methods, research, applications, opportunities and challenges. *Eng Struct*, 180: 332–348.

   https://doi.org/10.1016/j.engstruct.2018.11.045
3. Chen Z, Li Z, Li J, *et al*., 2019, 3D printing of ceramics: A review. *J Eur Ceram Soc*, 39: 661–687.
4. Sikder P, Ferreira JA, Fakhrabadi EA, *et al*., 2020, Bhaduri, bioactive amorphous magnesium phosphate-polyetheretherketone composite filaments for 3D printing. *Dent Mater*, 36: 865–883.
5. Daminabo SC, Goel S, Grammatikos SA, *et al*., 2020, thakur, fused deposition modeling-based additive manufacturing (3D printing): Techniques for polymer material systems. *Mater Today Chem*, 16: 100248.
6. Singh B, Kumar R, Chohan JS, 2020, Polymer matrix composites in 3D printing: A state of art review. *Mater Today*, 33: 1562–1567.
7. Ligon SC, Liska R, Stampfl J, *et al*., 2017, Polymers for 3D printing and customized additive manufacturing. *Chem Rev*, 117: 10212–10290.

   https://doi.org/10.1021/acs.chemrev.7b00074
8. Stansbury JW, Idacavage MJ, 2016, 3D printing with polymers: Challenges among expanding options and opportunities. *Dent Mater*, 32: 54–64.

   https://doi.org/10.1016/j.dental.2015.09.018
9. Wang X, Jiang M, Zhou Z, *et al*., 2017, 3D printing of polymer matrix composites: A review and prospective. *Compos Part B Eng*, 110: 442–458.

   https://doi.org/10.1016/j.compositesb.2016.11.034
10. Ortiz-Acosta D, Moore T, 2018, Functional 3D printed polymeric materials. In: Functional materials. 9: 1-5.

    https://doi.org/10.5772/intechopen.80686
11. Nadgorny M, Ameli A, 2018, functional polymers and nanocomposites for 3D printing of smart structures and devices. *ACS Appl Mater Interfaces*, 10: 17489–17507.
12. Falahati M, Ahmadvand P, Safaee S, *et al*., 2020, Smart polymers and nanocomposites for 3D and 4D printing. *Mater Today*, 40: 215–245.
13. Bekas D, Hou Y, Liu Y, *et al*., 2019, 3D printing to enable multifunctionality in polymer-based composites: A review. *Compos B Eng*, 179:107540.
14. Sagias V, Giannakopoulos KI, Stergiou CI, 2018, Mechanical properties of 3D printed polymer specimens. *Proc Struct Integr*, 10: 85–90.
15. Ahangar P, Cooke ME, Weber MH, *et al*., 2019, Current biomedical applications of 3D printing and additive manufacturing. *Appl Sci*, 9: 1713.
16. Fan D, Li Y, Wang X, *et al*., 2020, Progressive 3D printing technology and its application in medical materials. *Front Pharmacol*, 11: 122.

    https://doi.org/10.3389/fphar.2020.00122
17. Ahmed S, Chauhan VM, Ghaemmaghami AM, *et al*., 2019, New generation of bioreactors that advance extracellular matrix modelling and tissue engineering. *Biotechnol Lett*, 41: 1–25.

    https://doi.org/10.1007/s10529-018-2611-7
18. Pantazis AK, Papadakis G, Parasyris K, *et al*., 2020, 3D-printed bioreactors for dna amplification: Application to companion diagnostics. *Sens Actuators B Chem*, 319: 128161.

    https://doi.org/10.1016/j.snb.2020.128161
19. Ferraz MA, Henning HH, Da Costa PF, *et al*., 2018, Potential health and environmental risks of three-dimensional engineered polymers. *Environ Sci Technol Lett*, 5: 80–85.

    https://doi.org/10.1021/acs.estlett.7b00495
20. Inoue Y, Ikuta K, 2013, Detoxification of the photocurable polymer by heat treatment for microstereolithography. *Proc CIRP*, 5: 115–118.

    https://doi.org/10.1016/j.procir.2013.01.023
21. Campanale C, Massarelli C, Savino I, *et al*., 2020, A detailed review study on potential effects of microplastics and additives of concern on human health. *Int J Environ Res Public Health*, 17: 1212.

    https://doi.org/10.3390/ijerph17041212
22. Ojeda T, 2013, Polymers and the environment. *Polym Sci*, 23: 23.

    https://doi.org/10.5772/51057
23. Priyadarshini BM, Dikshit V, Zhang Y, 2020, 3D-printed bioreactors for *in vitro* modeling and analysis. *Int J Bioprint*, 6: 267.

    https://doi.org/10.18063/ijb.v6i4.267
24. Zhang Y, 2017, post-printing surface modification and functionalization of 3D-printed biomedical device. *Int J*

Bioprint, 3: 1.

https://doi.org/10.18063/IJB.2017.02.001

25. Popov VK, Evseev AV, Ivanov A, *et al*., 2004, Laser stereolithography and supercritical fluid processing for custom-designed implant fabrication. *J Mater Sci Mater Med*, 15: 123–128.

https://doi.org/10.1023/b: jmsm.0000011812.08185.2a

26. D'Urso PS, Effeney DJ, Earwaker WJ, *et al*., 2000, Custom cranioplasty using stereolithography and acrylic. *Br J Plast Surg*, 53: 200–204.

https://doi.org/10.1054/bjps.1999.3268

27. Putame G, Gabetti S, Carbonaro D, *et al*., 2020, Compact and tunable stretch bioreactor advancing tissue engineering implementation. application to engineered cardiac constructs. *Med Eng Phys*, 84: 1–9.

https://doi.org/10.1016/j.medengphy.2020.07.018

28. Rimington RP, Capel AJ, Chaplin KF, *et al*., 2019, Differentiation of bioengineered skeletal muscle within a 3D printed perfusion bioreactor reduces atrophic and inflammatory gene expression. *ACS Biomater Sci Eng*, 5: 5525–5538.

29. Banik BL, Brown JL, 2020, 3D-printed bioreactor enhances potential for tendon tissue engineering. *Regen Eng Transl Med*, 6: 1–10.

https://doi.org/10.1007/s40883-019-00145-y

30. Smith LJ, Li P, Holland MR, *et al*., 2018, FABRICA: A bioreactor platform for printing, perfusing, observing, and stimulating 3D tissues. *Sci Rep*, 8: 1–10.

31. Achinas S, Euverink GJ, 2019, Development Of An Anaerobic Digestion Screening System Using 3D-Printed Mini-Bioreactors. In: New Adv Ferment Processes. London: Intechopen.

32. Xia C, Fang NX, 2009, 3D microfabricated bioreactor with capillaries. *Biomed Microdev*, 11: 1309–1315.

https://doi.org/10.1007/s10544-009-9350-4

33. Zhou LY, Fu J, He Y, 2020, A review of 3D printing technologies for soft polymer materials. *Adv Funct Mater*, 30: 2000187.

https://doi.org/10.1002/adfm.202000187

34. Tamay DG, Usal TD, Alagoz AS, *et al*., 2019, 3D and 4D printing of polymers for tissue engineering applications. *Front Bioeng Biotechnol*, 7: 164–164.

https://doi.org/10.3389/fbioe.2019.00164

35. Tagliaferri V, Trovalusci F, Guarino S, *et al*., 2019, Environmental and economic analysis of fdm, sls and mjf additive manufacturing technologies. *Materials* (*Basel*), 12: 4161.

https://doi.org/10.3390/ma12244161

36. Calignano F, Galati M, Iuliano L, *et al*., 2019, design of additively manufactured structures for biomedical applications: A review of the additive manufacturing processes applied to the biomedical sector. *J Healthc Eng*, 2019: 9748212.

https://doi.org/10.1155/2019/9748212

37. Rahim TN, Abdullah AM, Akil HM, *et al*., 2016, Comparison of mechanical properties for polyamide 12 composite-based biomaterials fabricated by fused filament fabrication and injection molding. *AIP Conf Proc*, 1791: 020007

https://doi.org/10.1063/1.4968862

38. Feng L, Wang Y, Wei Q, 2019, PA12 powder recycled from SLS for FDM. *Polymers,* 11: 727.

https://doi.org/10.3390/polym11040727

39. Kinstlinger IS, Bastian A, Paulsen SJ, *et al*., 2016, Open-source selective laser sintering (OpenSLS) of nylon and biocompatible polycaprolactone. *PLoS One*, 11: e0147399

https://doi.org/10.1371/journal.pone.0147399

40. Shi Y, Pan T, Zhu W, *et al*., 2020, Artificial bone scaffolds of coral imitation prepared by selective laser sintering. *J Mech Behav Biomed Mater*, 104: 103664.

https://doi.org/10.1016/j.jmbbm.2020.103664

41. Gan X, Wang J, Wang Z, *et al*., 2019, Simultaneous realization of conductive segregation network microstructure and minimal surface porous macrostructure by SLS 3D printing. *Mater Des*, 178: 107874.

42. Hussain G, Khan WA, Ashraf HA, *et al*., 2019, Design and development of a lightweight SLS 3D printer with a controlled heating mechanism: Part A. *Int J Lightweight Mater Manuf*, 2: 373–378.

https://doi.org/10.1016/j.ijlmm.2019.01.005

43. Cai C, Tey WS, Chen J, *et al*., 2021, Comparative study on 3D printing of polyamide 12 by selective laser sintering and multi jet fusion. *J Mater Process Technol*, 288: 116882.

https://doi.org/10.1016/j.jmatprotec.2020.116882

44. Chin SY, Dikshit V, Priyadarshini BM, *et al*., 2020, Powder-based 3D printing for the fabrication of device with micro and mesoscale features. *Micromachines* (*Basel*), 11: 658.

https://doi.org/10.3390/mi11070658

45. Dikshit V, Goh GD, Nagalingam AP, *et al*., 2020, Recent progress in 3D printing of fiber-reinforced composite and nanocomposites. In: Han B, Sharma S, Nguyen TA, editors. Fiber-Reinforced Nanocomposites: Fundamentals and Applications. Ch. 17. Amsterdam: Elsevier, p371-p394.

46. Yuan S, Shen F, Chua CK, *et al*., 2019, Polymeric composites for powder-based additive manufacturing: Materials and applications. *Prog Polym Sci*, 91: 141–168.

https://doi.org/10.1016/j.progpolymsci.2018.11.001

47. Wu H, Fahy W, Kim S, *et al*., 2020, Recent developments in polymers/polymer nanocomposites for additive manufacturing. *Prog Mater Sci*, 111: 100638.

https://doi.org/10.1016/j.pmatsci.2020.100638

48. Wang H, Li Y, Zuo Y, *et al*., 2007, Biocompatibility and osteogenesis of biomimetic Nano-hydroxyapatite/polyamide composite scaffolds for bone tissue engineering. *Biomaterials*, 28: 3338–3348.

https://doi.org/10.1016/j.biomaterials.2007.04.014

49. Upadhyay DJ, Cui NY, Anderson CA, *et al*., 2004, A comparative study of the surface activation of polyamides using an air dielectric barrier discharge. *Colloids Surf Physicochem Eng Aspects*, 248: 47–56.

https://doi.org/10.1016/j.colsurfa.2004.08.016

50. Goodridge RD, Tuck CJ, Hague RJ, 2012, Laser sintering of polyamides and other polymers. *Prog Mater Sci*, 57: 229–267.

https://doi.org/10.1016/j.pmatsci.2011.04.001

51. Liu G, Li Y, Yang L, *et al*., 2017, Cytotoxicity study of polyethylene glycol derivatives. *RSC Adv*, 7: 18252–18259.

52. Yuan X, Zhang X, Sun L, *et al*., 2019, Cellular toxicity and immunological effects of Carbon-based nanomaterials. *Part Fibre Toxicol*, 16: 18.

53. Rosso S, Meneghello R, Biasetto L, *et al*., 2020, In-depth comparison of polyamide 12 parts manufactured by multi jet fusion and selective laser sintering. *Addit Manuf*, 36: 101713.

https://doi.org/10.1016/j.addma.2020.101713

54. Scherer B, Kottenstedde IL, Matysik FM, 2020, Material characterization of polyamide 12 and related agents used in the multi-jet fusion process: Complementary application of high-resolution mass spectrometry and other advanced instrumental techniques. *Monatsh Chem Chem Mon*, 151: 1203–1215.

55. Boyde A, Wood C, 1969, Preparation of animal tissues for Surface-scanning electron microscopy. *J Microsc*, 90: 221–249.

https://doi.org/10.1111/j.1365-2818.1969.tb00709.x

56. Ulmer K, Honjo S, 1973, Quantitative evaluation of fixation and dehydration methods for scanning electron microscopic preparation of soft sea water organisms. In: Proceeding 6th annual SEM symposium, p365.

57. Bessis M, Weed R, 1972, Preparation of red blood cells (RBC) for SEM. A survey of various artifacts. Scan *Electron Microsc*, 1: 290–296.

58. Waterman RE, 1972, Use of the scanning electron microscope for observation of vertebrate embryos. *Dev Biol*, 27: 276–81.

https://doi.org/10.1016/0012-1606(72)90103-0

59. Lin SD, Lamvik M, 1975, High resolution scanning electron microscopy at the subcellular level. *J Microsc*, 103: 249–257.

https://doi.org/10.1111/j.1365-2818.1975.tb03900.x

60. O'Connor HJ, Dickson AN, Dowling DP, 2018, Evaluation of the mechanical performance of polymer parts fabricated using a production scale multi jet fusion printing process. *Addit Manuf*, 22: 381–387.

https://doi.org/10.1016/j.addma.2018.05.035

61. Palma T, Munther M, Damasus P, *et al*., 2019, Multiscale mechanical and tribological characterizations of additively manufactured polyamide 12 parts with different print orientations. *J Manuf Processes*, 40: 76–83.

https://doi.org/10.1016/j.jmapro.2019.03.004

62. Dadbakhsh S, Verbelen L, Verkinderen O, *et al*., 2017, Effect of PA12 powder reuse on coalescence behaviour and microstructure of SLS parts. *Eur Polym J*, 92: 250–262.

https://doi.org/10.1016/j.eurpolymj.2017.05.014

63. Yusoff W, Thomas A, 2008, The effect of employing an effective laser sintering scanning strategy and energy density value on eliminating "Orange peel" on a selective laser sintered part. International association for management of technology, proceedings.

64. Holländer A, Cosemans P, 2020, Surface technology for additive manufacturing. *Plasma Processes Polym*, 17: 1900155.

https://doi.org/10.1002/ppap.201900155

65. Cai S, Wu C, Yang W, *et al*., 2020, Recent advance in surface modification for regulating cell adhesion and behaviors. *Nanotechnol Rev*, 9: 971–989.

https://doi.org/10.1515/ntrev-2020-0076

66. Wieslander AP, Nordin MK, Hansson B, *et al*., 1993, *In vitro* toxicity of biomaterials determined with cell density, total protein, cell cycle distribution and adenine nucleotides. *Biomater Artif Cells Immobilization Biotechnol*, 21: 63–70.

https://doi.org/10.3109/10731199309118297

67. Kumar P, Nagarajan A, Uchil PD, 2018, Analysis of cell viability by the MTT assay. *Cold Spring Harb Protoc*, 2018: pdb.prot095505.

68. Alimohamadi M, Ownagh V, Mahouzi L, *et al*., 2014, The impact of immunohistochemical markers of ki-67 and p53 on the Long-term outcome of growth Hormone-secreting pituitary adenomas: A cohort study. *Asian J Neurosurg*, 9:130–136.

https://doi.org/10.4103/1793-5482.142732

69. El Badawi ZH, Muhammad EM, Noaman HH, 2015, Utility of Ki-67 labeling index in the differential diagnosis of osteogenic bone tumors. *Al-Azhar Assiut Med J*, 13: 1687–1693.

70. Yan XZ, Yang W, Yang F, *et al*., 2014, Effects of continuous passaging on mineralization of MC3T3-E1 cells with improved osteogenic culture protocol. *Tissue Eng Part C Methods*, 20: 198–204.

https://doi.org/10.1089/ten.tec.2012.0412

71. Liao H, He H, Chen Y, *et al*., 2014, Effects of Long-term serial cell passaging on cell spreading, migration, and Cell-surface ultrastructures of cultured vascular endothelial cells. *Cytotechnology*, 66: 229–238.

https://doi.org/10.1007/s10616-013-9560-8

72. Hughes FJ. 1998, Aubin JE, 1998, Culture of cells of the osteoblast lineage. *Methods Bone Biol*, 22: 1–49.

73. Thio BJ, Meredith JC, 2008, Quantification of *E. coli* adhesion to polyamides and polystyrene with atomic force microscopy. *Colloids Surf B Biointerfaces*, 65: 308–312.

https://doi.org/10.1016/j.colsurfb.2008.05.005

74. Wang H, Feng H, Liang W, *et al*., 2009, Malyarchuk, effect of surface roughness on retention and removal of *Escherichia coli* O157: H7 on surfaces of selected fruits. *J Food Sci*, 74: E8–E15.

https://doi.org/10.1111/j.1750-3841.2008.00998.x